

## The Mechanical Response of Gold Substrates Passivated by Self-Assembling Monolayer Films

Ross C. Thomas, J. E. Houston, Terry A. Michalske, Richard M. Crooks

Interfacial force microscopy has been used to show that a single layer of self-assembling molecules adsorbed on a gold substrate can prevent adhesion between gold and a tungsten probe. The passivated gold is able to elastically support large repulsive loads, with plots of load versus deformation closely following the Hertzian model. The gold shear-stress threshold for plastic deformation is determined to be  $\sim 1$  gigapascal, which is in agreement with the theoretical value for the intrinsic gold-lattice stability.

In this report, we expand our earlier interfacial force microscopy (IFM) studies (1, 2) to quantitatively evaluate how a thin, organized monolayer film changes the mechanical interaction between a Au surface and a W IFM probe. Specifically, we show that below substrate shear-stress levels of  $\sim 1.0$  GPa, the deformations are consistent with those expected from a Hertzian model involving a rigid, noninteracting punch elastically deforming a planar substrate. For higher stress levels, the surface is found to permanently deform. However, the passivating properties of the film are maintained even after considerable plastic deformation. This behavior is in stark contrast to the situation observed in the absence of the monolayer film, where we find that permanent damage occurs under negligible loads and that Au is transferred to the probe surface.

We prepared the monolayer films by soaking Au substrates in 0.5 mM *n*-docosaneithiol [ $\text{CH}_3(\text{CH}_2)_{21}\text{SH}$ ] solutions in purified hexadecane for 24 hours. Substrates were prepared by electron-beam vapor deposition of 20 nm of Ti followed by 200 nm of Au onto Si(100) surfaces. Immediately before adsorbing the organic films, the Au substrates were cleaned in a 3:1 concentrated solution of  $\text{H}_2\text{SO}_4$  and a 30%  $\text{H}_2\text{O}_2$  solution. Freshly prepared monolayer surfaces were thoroughly rinsed with hexadecane and dried with  $\text{N}_2$ . The films were characterized by ellipsometry and Fourier transform infrared external reflectance spectroscopy before IFM studies. The thickness and vibrational spectra agreed with those reported previously (3, 4).

The IFM (5) measurements were carried out in a low-pressure chamber evacuated to  $10^{-8}$  torr and backfilled with dry  $\text{N}_2$ . The W probe was characterized by scanning electron microscopy (SEM) and found to

have a parabolic shape with an apex radius of curvature  $\sim 500$  nm. We obtained IFM loading data in the force-feedback mode by bringing the sample from probe-sample separations of a few nanometers into repulsive contact up to a specified load level and then returning it to the original position at a constant rate of 5 nm/s. Force images were taken in the repulsive mode (without feedback) at a constant load level of  $0.2 \mu\text{N}$ .

A typical loading cycle for an *n*-docosaneithiol film is shown in Fig. 1A up to repulsive loads of almost  $15 \mu\text{N}$ . (Positive displacements indicate repulsive forces.) The zero separation value is arbitrarily chosen to represent the starting point of the sample approach. In agreement with our earlier results involving a hexadecaneithiol [ $\text{CH}_3(\text{CH}_2)_{15}\text{SH}$ ] film (1, 2), several features are evident from these results. (i) Negligible attractive behavior is detected at any point in the cycle. (ii) A hysteresis loop develops after film contact (closing after a small displacement of  $\sim 2.5$  nm), which results from the anelastic response of the film being compressed between the probe and substrate surface. (iii) The loop closes at higher loads, which indicates a fully compressed film with the observation of further deformation representing the elastic response of the substrate surface.

Because no evidence of an adhesive interaction is seen in Fig. 1A, the loading behavior can be analyzed by a simple Hertzian model (6) that consists of a noninteracting, rigid parabolic punch deforming an elastic half-space. Such a model indicates that after contact, the applied load will scale as the three-halves power of the displacement (6). The unloading portion of Fig. 1A is shown in Fig. 1B along with a Hertzian model curve. Only the unloading portion of the cycle of Fig. 1A is shown because it is least affected by the mechanical properties of the film (1). We obtained the model curve by performing a least squares fit to an offset origin, three-halves power function over the region from 4 to 5.6 nm to determine both the origin-offset value and the prefactor for the Hertzian

equation (6). This approach allowed us to plot by analytic continuation the resulting model function down to the contact point.

The excellent fit of the Hertzian model function over a large portion of the unloading curve in Fig. 1B lends credibility to the purely elastic contact-mechanics model and permits a determination of the probe-tip dimensions and the contact stresses in the substrate. Following this approach (6), we calculate the parabolic-tip radius of curvature to be  $\sim 375$  nm and the load of  $15 \mu\text{N}$  to represent a maximum compressive stress of  $\sim 3.4$  GPa. Subsequent continuum-elasticity analysis indicates that this loading condition results in a maximum substrate shear stress of  $\sim 1.0$  GPa (7).

We can determine the threshold stress level for plastic deformation by taking load-cycle data of the kind shown in Fig. 1 to higher loading levels. Figure 2A shows data taken in the same region as data in Fig. 1A up to a peak load of  $27 \mu\text{N}$ . In contrast to Fig. 1A, hysteresis is observed over the entire loading cycle, which indicates that plastic deformation has occurred. We can estimate the loading threshold for plastic deformation by comparing the measured loading curve with that predicted by the elastic analysis (Fig. 1B). The comparison is shown in Fig. 2B, where the point-of-contact has been shifted to compensate for the different starting point for the loading cycle. The substrate loading behavior follows the model function over only a limited region (deviating at the higher loading levels), which indicates a threshold for plastic deformation near  $15 \mu\text{N}$ . This load

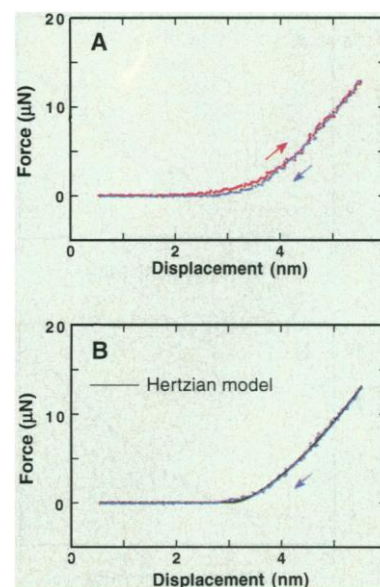


**Fig. 1.** (A) Loading-cycle behavior for a Au surface covered by a  $\text{CH}_3(\text{CH}_2)_{21}\text{SH}$  monolayer film interacting with a W probe. (B) Withdrawal curve of the loading cycle in (A) compared with a Hertzian model function (7).

R. C. Thomas and R. M. Crooks, Department of Chemistry, University of New Mexico, Albuquerque, NM 87131.

J. E. Houston and T. A. Michalske, Surface Science Department, Sandia National Laboratories, Albuquerque, NM 87185.

was determined to represent a maximum shear stress of  $\sim 1.0$  GPa.

We can directly verify the deformation of the Au substrate by repulsive-force imaging. Figure 3, A and B, shows such images taken before and after, respectively, a loading cycle to  $57 \mu\text{N}$ . The surface defect in the upper left of each panel serves as a reference point for the evaluation of instrumental drift during the  $\sim 10$ -min data acquisition period.

The indentation can clearly be seen in the image of Fig. 3B. However, the details of the shape of the deformed area are better illustrated by subtracting the first image from the second (Fig. 3C). Treating the data in this manner eliminates the general surface morphological structure as well as the defect in the upper left of Fig. 3, A and B, and confirms the stability of the instrument. Line scans through the center of the deformed area indicate that the deformation has a width and depth of approximately 51 and 2.8 nm, respectively, which results in a calculated parabolic-tip radius of 460 nm. This value is in good agreement with the SEM results and our Hertzian deformation analysis.

To underscore the role of the film in the behavior shown in Figs. 1 and 2, we show in Fig. 4A the contrasting results for a W probe interacting with a Au surface in the absence of the thiol film. We prepared the substrate by cleaning it in a 3:1 concentrated solution of  $\text{H}_2\text{SO}_4$  and a 30%  $\text{H}_2\text{O}_2$  solution immediately before imaging. For this surface, we observe a slight repulsive wall at a relative displacement of  $\sim 48$  nm that we attribute to

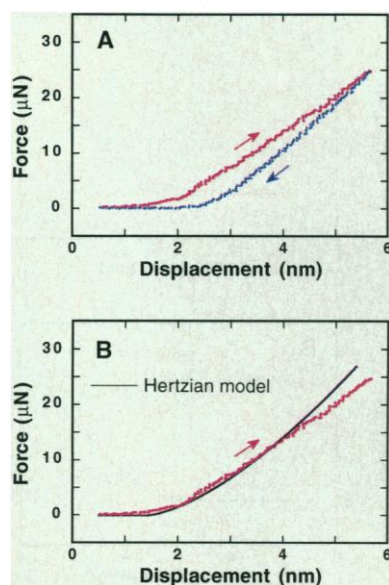


**Fig. 2.** (A) Loading-cycle measurement for a monolayer-covered Au substrate up to a repulsive load of  $\sim 27 \mu\text{N}$ . (B) Data obtained from the approach portion in (A) plotted against the Hertzian model function obtained in Fig. 1B.

probe contact with a layer of surface contamination, probably consisting of adventitious hydrocarbons and water (8). At a repulsive load near  $0.4 \mu\text{N}$ , the probe begins to displace the contaminant layer and develop an adhesive substrate bond (9). The adhesive force rapidly rises to  $\sim -1 \mu\text{N}$  and then, after probe-substrate contact, turns repulsive at  $\sim 33$  nm.

Upon the reversal of the sample motion, hysteresis immediately develops and a significant adhesive bond is formed that reaches levels of  $\sim -3 \mu\text{N}$  near a displacement of 29 nm. Subsequently, the adhesive contact ruptures and the interfacial force returns to zero. Rupture occurs near the point of original contact, which indicates that the strong adhesive interaction has resulted in a considerable flow of Au toward the probe as it is withdrawn, forming a neck that narrows and eventually fails. This "galling" behavior is very similar to that found in clean-surface modeling of metal-probe, metal-substrate interactions (10).

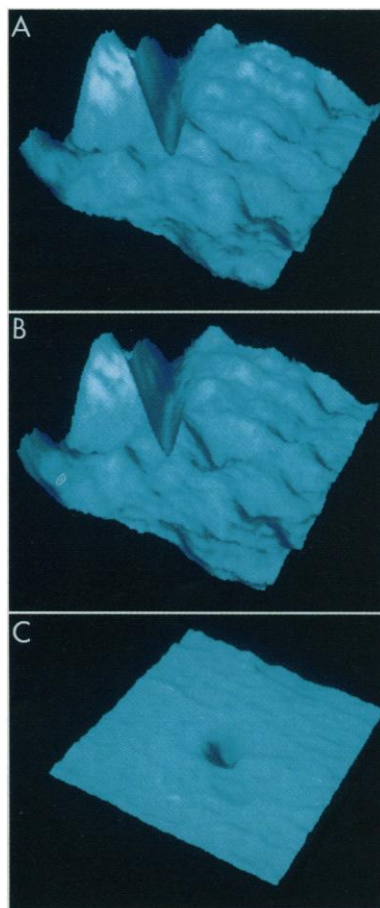


**Fig. 3.** Constant repulsive-force images of Au covered by a  $\text{CH}_3(\text{CH}_2)_{21}\text{SH}$  monolayer film. (A) Image before loading-cycle data. (B) Image taken after a loading cycle to a peak load of  $57 \mu\text{N}$ . (C) A difference image resulting from subtracting the image in (B) from that in (A). The relative height scales have been magnified ten times.

We can visualize the galling effect of the tip-substrate interaction by repulsive-force imaging as illustrated in Fig. 4B. The  $0.2\text{-}\mu\text{N}$  repulsive load is insufficient to break through the contaminant layer (Fig. 4A) and permits imaging without galling. The general morphological structure of the polycrystalline surface can be seen along with several distinct depressions not present in the original surface. Line scans reveal a height relief of the depressions of several nanometers and widths of several tens of nanometers.

The sides of the depressions are steep, which supports the notion that large chunks of Au have been torn from the substrate surface during the process of neck formation and rupture described above. In support of this contention, we find that the general resolution of images taken after the loading cycle is enhanced, which indicates that the morphological structure of the probe has been altered (sharpened). One can regain the original image quality by field-desorbing Au from the probe surface because it has a low desorption field strength (11). The procedure can be repeated with similar results, which provides compelling evidence for Au transfer.

As a result of the stable, quantitative nature of IFM, we have been able to determine the threshold stress value for the

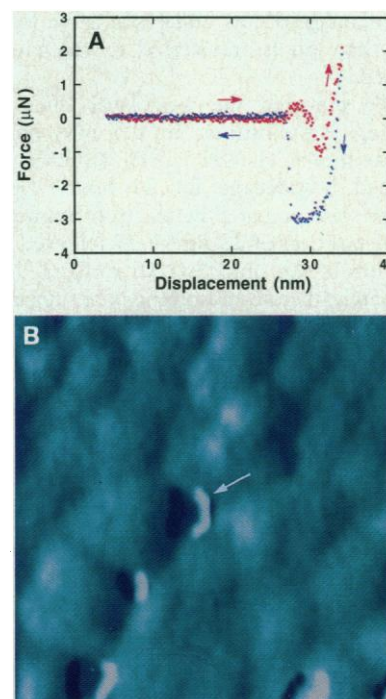


**Fig. 4.** (A) Loading cycle for a Au substrate interacting with W in the absence of the monolayer film. (B) Constant repulsive-force image (300 by 300 nm) of the Au surface after the loading cycle of (A). The relative height scale has been magnified ten times. Arrow denotes one of several distinct depressions.

plastic deformation of a Au surface passivated by a self-assembling monolayer film. The shear-stress value of  $\sim 1$  GPa agrees remarkably well with the 0.74-GPa figure calculated for the intrinsic Au lattice (12). It has long been recognized that an adhesive interaction between probe and substrate in indenter experiments can have a dramatic effect on the measured contact-deformation results (13). The interaction gives rise to an enhanced production of defects in the high-stress region near the edges of the contact area, which results in plastic deformation under reduced loading. The effect has been dramatically illustrated by recent model calculations (10). Furthermore, it is known that oxide and carbon contamination films of greater than  $\sim 5$ -nm thickness on metal surfaces can cause large changes in indenter behavior (14). However, these films can produce such effects as a result of their own mechanical properties. In contrast, one monolayer of molecules, interacting with one another through van der Waals forces, is not expected to support significant levels of shear stress. Thus, it is the monolayer film's ability to passivate the interfacial adhesion interaction that is primarily responsible for our being able to measure plastic shear-stress thresholds near the theoretical limit.

Passivating films, such as the alkanethiols used here, that are stable under high loads can be important in surface mechanical property studies of materials and show great potential for aiding in understanding the role of the interface in defect production and migration. These attributes are, of course, in addition to the function of passivating films as highly breakdown-resistant, surface-specific lubricants.

## REFERENCES AND NOTES

1. S. A. Joyce, R. C. Thomas, J. E. Houston, T. A. Michalske, R. M. Crooks, *Phys. Rev. Lett.* **68**, 2790 (1992).
2. J. E. Houston and T. A. Michalske, *Nature* **356**, 266 (1992).
3. L. H. Dubois and R. G. Nuzzo, *Annu. Rev. Phys. Chem.* **43**, 437 (1992).
4. M. D. Porter, T. B. Bright, D. L. Allara, C. E. D. Chidsey, *J. Am. Chem. Soc.* **109**, 3559 (1987).
5. S. A. Joyce and J. E. Houston, *Rev. Sci. Instrum.* **62**, 710 (1991).
6. I. N. Sneddon, *Int. J. Eng. Sci.* **3**, 47 (1965).
7. S. P. Timoshenko and J. N. Goodier, *Theory of Elasticity* (McGraw-Hill, New York, 1970).
8. N. A. Burnham and R. J. Colton, *J. Vac. Sci. Technol. A* **7**, 2906 (1989).
9. This process is described by U. Landman, W. D. Luedtke, and E. M. Ringer [*Wear* **153**, 3 (1992)] in detailed theoretical modeling of a Ni tip interacting with a Au surface covered by *n*-hexadecane molecules.
10. U. Landman, W. D. Luedtke, N. A. Burnham, R. J. Colton, *Science* **248**, 454 (1990).
11. T. T. Tsong, *Atom-Probe Field Ion Microscopy* (Cambridge Univ. Press, New York, 1990), chap. 2.
12. A. Kelley and N. H. Macmillan, *Strong Solids* (Clarendon, Oxford, 1986).
13. K. L. Johnson, K. Kendall, A. D. Roberts, *Proc. R.*

*Soc. London Ser. A* **324**, 301 (1971); B. V. Derjaguin, V. M. Muller, Yu. P. Toporov, *J. Colloid Interface Sci.* **53**, 2 (1975).

14. D. Pashley, J. B. Pethica, D. Tabor, *Wear* **100**, 7 (1984); N. Gane, *Proc. R. Soc. London Ser. A* **317**, 367 (1970).
15. The authors wish to thank S. A. Joyce for his many helpful discussions. R.C.T. acknowledges the support of Associated Western Universities

through a Department of Energy laboratory graduate fellowship. J.E.H. and T.A.M. acknowledge support by the Office of Basic Energy Sciences Division of Material Sciences, Department of Energy, under contract DE-AC04-76DP00789. R.M.C. acknowledges the support of the Office of Naval Research (Young Investigator Program).

13 October 1992; accepted 26 January 1993

## C<sub>60</sub>H<sub>2</sub>: Synthesis of the Simplest C<sub>60</sub> Hydrocarbon Derivative

Craig C. Henderson and Paul A. Cahill\*

The reaction of C<sub>60</sub> with BH<sub>3</sub>:tetrahydrofuran in toluene followed by hydrolysis yielded C<sub>60</sub>H<sub>2</sub>. This product was separated by high-performance liquid chromatography and characterized as the addition product of H<sub>2</sub> to a 6,6-ring fusion (1a1b isomer). The <sup>1</sup>H nuclear magnetic resonance (NMR) spectrum of the product remained a sharp singlet between  $-80^\circ$  and  $+100^\circ\text{C}$ , which suggests a static structure on the NMR time scale. Hydrolysis of the proposed borane addition product with acetic acid-*d*<sub>4</sub> or D<sub>2</sub>O yielded C<sub>60</sub>HD, and its <sup>3</sup>J<sub>HD</sub> coupling constant is consistent with vicinal addition. The observation of a single C<sub>60</sub>H<sub>2</sub> isomer is in complete agreement with earlier calculations that indicated that at most 2 of the 23 possible isomers of C<sub>60</sub> would be observable at equilibrium at room temperature. These results suggest that organoborane chemistry may be applied to further functionalization of fullerenes.

The synthesis of macroscopic amounts of C<sub>60</sub> has generated much interest in the physical and chemical properties of this spherical molecule (1). Fully characterized synthetic derivatives of C<sub>60</sub> have largely been limited to the epoxide, C<sub>60</sub>O (2), C<sub>60</sub>CR<sub>2</sub> fulleroids (3) and related compounds, osmate esters (4), polybrominated derivatives (5), and organometallic compounds, including several iridium (6) and platinum (7) complexes. The dihydride derivative is somewhat different from many known derivatives because the hydrogen atoms would, in principle, be free to add to any two carbon atoms.

We had previously studied C<sub>60</sub>H<sub>2</sub> computationally to gain insight into which, if any, of the 23 isomers of C<sub>60</sub>H<sub>2</sub> would be preferentially populated at equilibrium at room temperature (8). A nomenclature system (8) was devised for enumerating these isomers (it appears in slightly revised form in Fig. 1), in which C<sub>60</sub> is composed of eight layers, labeled a, b, c, d, d', c', b', and a', in a manner that emphasizes the symmetry of this molecule. Each carbon atom in a given layer is then labeled numerically to identify it uniquely. Addition of functional groups, such as H<sub>2</sub> addition to a 6,6 or 6,5 ring fusion is then identified by the carbon label, for example, 1a,1b-C<sub>60</sub>H<sub>2</sub> or 1a,2a-C<sub>60</sub>H<sub>2</sub>, respectively. Semiempirical calculations suggested that the 1a1b and

1a2c isomers of C<sub>60</sub>H<sub>2</sub> have the lowest heats of formation, with the 1a2c isomer (1,4 addition across a 6-ring) having a heat of formation 3.8 kcal/mol higher in energy. Similar calculations on the 143 isomers of C<sub>70</sub>H<sub>2</sub> indicate that four isomers, 1c2c, 1a1b, 1a2c, and 1d10d', have the lowest heats of formation (9).

The synthesis, separation, and characterization of C<sub>60</sub>H<sub>2</sub> appeared reasonable, given these computational results. Methods of reducing C<sub>60</sub> to yield polyhydride mixtures have been published (10), and several other standard reduction approaches are

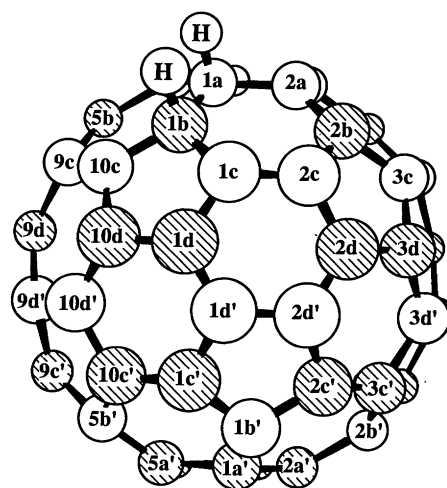


**Fig. 1.** Structure of the observed 1a1b isomer of C<sub>60</sub>H<sub>2</sub> showing the proposed nomenclature system for addition products of C<sub>60</sub>. A similar system for C<sub>70</sub> includes an "e" equatorial layer.

Department 1811, Sandia National Laboratories, Albuquerque, NM 87185.

\*To whom correspondence should be addressed.